04,09,12,13

Photoluminescence and electron paramagnetic resonance of ultrathin layers of nanosized porous silicon

© E.S. Demidov[1], D.A. Afanasev[1], N.E. Demidova[2], A.V. Nezhdanov[1], A.I. Mashin[1]

[1] Lobachevsky State University,
Nizhny Novgorod, Russia
[2] Nizhny Novgorod State University of Architecture and Civil Engineering,
Nizhny Novgorod, Russia

E-mail: demidov@phys.unn.ru

Received August 23, 2025
Revised October 24, 2025
Accepted November 20, 2025

For the first time the change of photoluminescence and electron paramagnetic resonance with increase in time of electrochemical formation of nanosized porous silicon since ultrathin layers on monocrystal Si plates *p*- and n^+-type is experimentally investigated. Thus, for both variants of Si the red shift of photoluminescence spectra is revealed. The quantum-dimensional model as mechanism of cascade growth of porous silicon layers and the photoluminescence red shift is offered. According to electron paramagnetic resonance data of no radiating recombination P_b — centers the growth of silicon nanosized inclusions mass with porous silicon layer thickness on Si-n^+ is established close to linear. Possibility of working out actual today manufacturing techniques from porous silicon of system silicon nanowires, immersed in the dielectric environment, is discussed.

Keywords: Anode etching, porous silicon, ultrathin layers, photoluminescence, electron paramagnetic resonance, dimensional quantization, silicon nanowires.

DOI: 10.61011/PSS.2026.01.63238.238-25

1. Introduction

For various promising applications of porous silicon (PS) listed in Refs. [1–4], information about changes in the morphology and structure of this material with increasing thickness of porous layers is important. A generally accepted condition for the reaction of anodic pore formation in a hydrofluoric acid solution is the possibility of holes entering from bulk silicon to its surface [1, p. 10]. The common feature of PS layers on *n*- and *p*-type silicon is an increase in porosity with increasing time of their formation and current density of anode etching [1, p. 13]. The mechanism of pore formation and their modification in the process of anodic etching of silicon has been developed in the most detail for the case of macroporous PS, when the pore diameter exceeds 50 nm [5–7]. In particular, in this theory, an increase in pore length as anodic etching continues is associated with the highest electric field intensity in the region of the pore bottom. The cessation of the elongation of part of the pores is explained by the blocking accumulation of hydrogen ions at the bottom of the pore.

To determine the mechanism of layer growth of nanoscale PS layers with a pore diameter and a distance between them in units of nanometers (mesoporous silicon in the terminology [8,9]), experimental data on changes in the properties of this material are currently lacking, starting from the early stage of the kinetics of formation of ultrathin PS films. Strangely enough, despite the very large number of publications on PS, the change in photoluminescence (PL) spectra with increasing thickness of ultrathin layers of nanoscale PS has not been studied at all. Regarding other PS properties, there is only one work [10], in which, using X-ray reflectometry (XRR), the authors studied the change in the properties of ultrathin PS layers as the *p*-type silicon ($3-6\,\Omega\cdot$cm) was anodically etched from 10 s to 100 s, which corresponded to an increase in the thickness of the porous layer from 40 nm to 380 nm. An important result was obtained, and in the case of ultrathin layers, as the PS layer thickened, its porosity increased (from 46 % to 75 %). This paper presents data on measurements of PL and electron paramagnetic resonance (EPR) spectra as a function of the time of anodic PS formation, starting with ultrathin porous layers on *p*- and n^+-type silicon crystals in HF:C_2H_5OH solution. At the same time, a redshift of the PL spectra was detected for both Si variants. A quantum-dimensional model of both the mechanism of growth of porous silicon layers and the redshift of FL is proposed. According to the results of EPR of the well-known P_b-centers of nonradiative recombination [1], a close to linear increase in the proportion of silicon nanoparticles in PS was found with an increase in the thickness of the porous layer on Si-n^+.

2. Experimental samples and methods

Porous layers were electrochemically formed on single crystal silicon wafers of industrial grades KES-0.01 with a resistivity of $0.01\,\Omega\cdot$cm and orientation (111) and KDB-2

with a resistivity of $2\,\Omega \cdot$ cm and orientation (111) in a mixture of 55% hydrofluoric acid HF and ethyl alcohol C_2H_5OH in a ratio of 1:1 at an average current density of 10 mA/cm^2. The PS formation time t_f varied from 6 s to 600 s. PS layers with a thickness of $\approx 1\,\mu$m were formed on silicon KDB-2 and $\approx 2\,\mu$m on KES-0.01 in 600 s according to spherical slice data or measurements using the LEF-3M-1 ellipsometer. An uneven scale of growth of t_f was applied with the smallest step of change of this parameter at the beginning, in the range of the main interest of the study — ultrathin PS layers. The silicon wafers were mechanically and chemically polished before forming the PS layers. The samples were washed twice in ethyl alcohol after anodic etching. PL spectra were studied at room temperature using the NTEGRA Spectra Raman spectroscopy complex manufactured by NT-MDT (Zelenograd) with a 473 nm laser and a silicon CCD matrix cooled to -55°C as a detector. The EPR spectra were recorded using a 3 cm EMX 10/12 spectrometer manufactured by Brooker at 293 K. Before the measurements, the samples were stored in the air for about two weeks.

3. Results and discussion

Figure 1 shows the PL spectra of PS samples on KDB-2 at 293 K for different formation times of porous layers in the range of t_f from 6 to 120 s, corresponding to ultrathin PS layers with a thickness of d_{PS} from 10 to 200 nm, and further up to 1000 nm. As can be seen, it was possible to observe the PL of PS samples with a change in the formation time by two orders of magnitude.

The dependences of the position of the maximum λ_{max}, the line width of the spectrum $\Delta\lambda$ at half-height, and the intensity at the maximum I_{max} of the PL spectrum on t_f of layers of PS on KDB-2 single crystals obtained from spectra on Figure 1 are shown in Figure 2. Solid trend curves show that, on average, there is a red shift of 100 nm of the PL maximum λ_{max} (Figure 2, *a*), $\sim 5\%$ increase in the width of the spectrum line $\Delta\lambda$ (Figure 2, *b*) and a close to parabolic growth of $I_{max} \sim t_f^2$ as the thickness of the porous layer increases (Figure 2, *c*). The measured PL maximum change interval of the PS λ_{max} in Figure 1 is located in the long-wavelength part of the well-known S-band 400–800 nm [1,2,11], which is described by a model of quantum confinement or dimensional quantization.

We take into account the phenomenon of dimensional quantization to explain both PL and the formation of a nanoscale PS. The quantum-dimensional PL model is proposed in Ref. [9]. As in Ref. [9], we use an idealized top view of the PS layer formed before oxidation (shown in Figure 3, *a*). Here R is the pore radius, L is the distance between the pore centers, h is the minimum silicon wall thickness between adjacent pores. We have added a view of oxidized PS to this pattern, as in Ref. [12] in Figure 3, *b*. It is known that natural silicon oxide with a thickness of 2–5 nm grows in air at room temperature on the flat

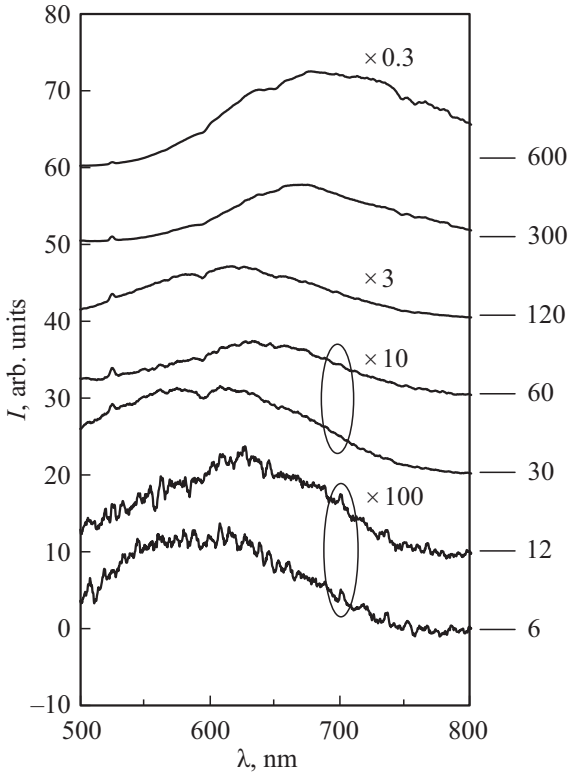

Figure 1. PL spectra of PS samples on KDB-2 at 293 K for different formation times t_f, shown by numbers on the right in seconds.

surface of a silicon single crystal. In a PS exposed to air, as the inner walls of the pores oxidize, from a certain point in time, the oxide inner environments of the pores close together and the remaining parts of the non-oxidized silicon in the PS turn out to be silicon filaments (quantum wires) with a transverse size of units of nanometers. The value of d is the thickness of the oxide layer inside the pore in Figure 3, *b*. Since the volume of the formed silicon oxide is approximately twice the volume of the initial silicon, the former pore cross-section boundary runs approximately in the middle of the oxide layer in each pore, as shown by the dotted line in Figure 3, *b*. The silicon — silicon oxide system tends to minimize the free energy achieved by minimizing the length of the boundary between these two phases, i.e., the energetically unfavorable cross-section of silicon filaments in the form of squares with concave sides is replaced by a circular cross-section with the same area as in Figure 3, *c*. The transverse size of the silicon filaments determines the wavelength λ_{max} of the PL maximum [11,13] and the range λ_{max} in Figure 2, *a* 600–700 nm according to Ref. [11] corresponds to a thread diameter of about 2 nm.

There are the following relations between the parameters in Figure 3. The distance between the pore centers $L = 2R + h$, $(2R + h)^2 = L^2$ is the cross-sectional area of one lattice cell of the periodic pore structure, porosity in fractions of a unit $P = \pi R^2/L^2$. Taking into account these ratios, the radius of the silicon filament in Figure 3, *c* is

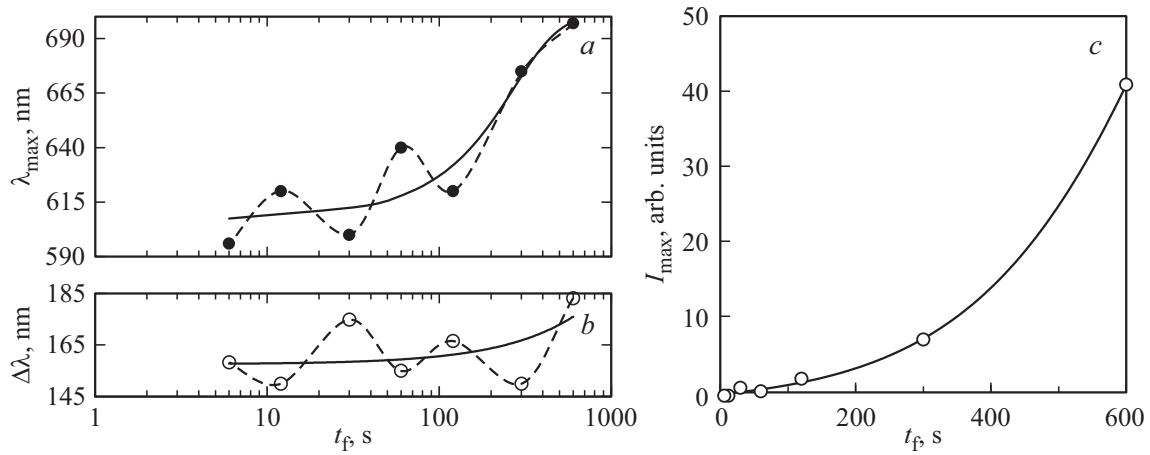

Figure 2. Dependences of the parameters of the PL spectra at 293 K on the formation time t_f of PS layers on single crystals KDB-2: *a* — positions of the PL maximum λ_{max}, *b* — spectral widths $\Delta\lambda$, *c* — maximum PL intensity I_{max}. Solid curves show trend lines. The dotted line on the charts *a* and *b* indicates deviations of the experimental points from the trend line.

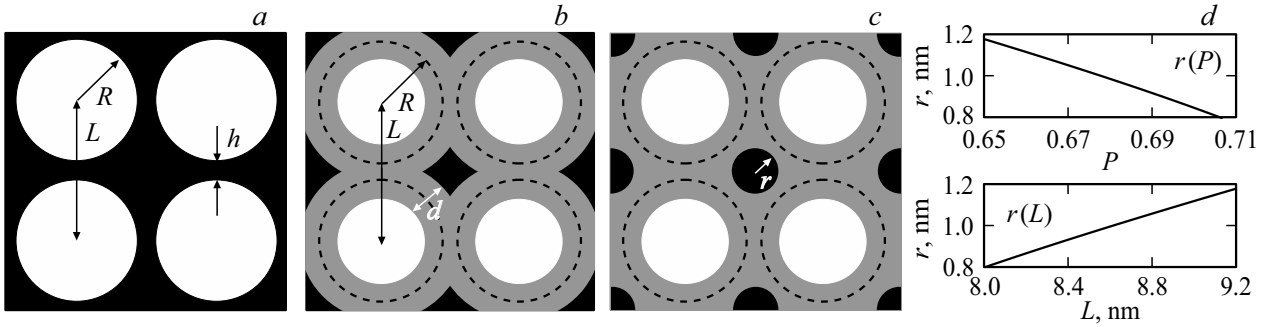

Figure 3. Idealized top view of the layer *a* — an original PS with a porosity of about 65 % before oxidation, *b* — an oxidized PS as in Ref. [11] with the formation of silicon filaments and *c* — an oxidized PS with silicon filaments of circular cross section (here on the fragments *a*–*c* white — air, gray — silicon oxide, black — silicon); *d* — formula (1) defined trends in changes in the radius of the silicon filament $r(P)$ with increasing porosity P at fixed oxide layer thicknesses $d = 2.5$ nm and the distance between the pore centers $L = 9.6$ nm or the radius of the silicon filament $r(L)$ with increasing distance between pores L at fixed $d = 2.5$ nm and minimum silicon wall thickness $h = 1.0$ nm between adjacent pores (Figure 3, *a*).

determined by the formula

$$r = \sqrt{\frac{4L^2 + 16Ss - \pi(L - h + d)^2}{4\pi}}, \qquad (1)$$

where

$$Ss = \frac{(L-h)^2}{8}\left(2\arccos\left(\frac{L-d}{L-h}\right) - \sin\left(2\arccos\left(\frac{L-d}{L-h}\right)\right)\right).$$

According to X-ray reflectometry data [10], the porosity increases P with increase of the thickness of the ultrathin porous layer. At the same time, as shown in Figure 3, *d*, with increasing porosity P with a constant distance between the pore centers L after PS oxidation, the radius of the silicon filament $r(P)$ decreases ($r(P)$ in Figure 3, *d*) due to an increase in the pore radius by the ratio $P = \pi R^2/L^2$, i.e., there should be a blue shift of PL, which contradicts the experimentally observed red shift in Figure 2, *a*. A red shift of PL with increasing porosity is possible if, with increasing time of PS formation, if the distance between the pores increases, which leads to an increase in the radius of silicon filaments (see $r(L)$ in Figure 3, *d*). Here, as in the case of the formation of macropores [5–7], it is likely that the elongation of part of the pores will be stopped by the blocking accumulation of hydrogen ions at the bottom of the pore. As a result, the average distance between pores increases, and after PS oxidation, the average transverse size of silicon filaments increases, leading to a red shift of PL. It should be noted that an increase in the average distance between the pores as a result of the fusion of two neighboring pores is hardly possible. If the distance between the pores in the thin wall is too close, due to the quantum-dimensional increase in the barrier for holes, their entry into this region is sharply limited, which stops the reaction of anodic etching of silicon in this place and the destruction of the wall between the pores. A quantum-dimensional mechanism of pore curvature, an increase in their diameter, and an

equalization of the distances between them is likely after the elongation of part of the pores has stopped. For example, in regions with an increased distance between neighboring pores, the quantum-dimensional barrier for holes is lowered, which favors their increased entry into this place. This contributes to the curvature and convergence of the pores by expanding the pores towards the neighboring outermost pore. The outermost neighboring pores are „attracted“ more strongly.

The dotted non-monotonic curve on Figure 2, *a* indicates the deviation of the experimental points $\lambda_{\max}$ from the trend line, which significantly exceeds the measurement error and noise level. Of course, this is an approximate experimental dependence $\lambda_{\max}(t_f)$, since there are not enough intermediate points. It is important that there are alternating intervals with a red and blue shift of the PL peak relative to the trend line. According to the scheme of the structure of oxidized PS in Figure 3, *c*, there is a cascade of approximately identical pores growing in length and diameter in the blue shift region, and there are no pores falling out due to hydrogen passivation. As a result of oxidation, silicon filaments are thinned ($r(P)$ in Figure 3, *d*) and $\lambda_{\max}$ shifts towards lower values. Then comes the stage of dilution of the pore density due to hydrogen passivation of part of the pores and the deviation of $\lambda_{\max}$ towards higher values ($r(L)$ in Figure 3, *d*). And these stages or cascades of elongation and subsequent dilution of pore density according to Figure 2, *a* are repeated. The antiphase to $\lambda_{\max}$ fluctuations in the PL spectrum width $\Delta\lambda$ in Figure 2, *b* are explained by the fact that at the stage of cascade formation, for example, the PL spectrum is broadened in the range of t_f from 12 to 30 s as a result of the superposition of the spectrum from the regions between the stopped pores from $\lambda_{\max} = 620$ nm at the previous stage from 6 to 12 s and the spectrum from the regions between the pores in the cascade with a blue shift to $\lambda_{\max} = 600$ nm. Probably, the initial section of the red shift from $t_f = 6$ s to 12 s in Figure 2, *a* is preceded by a cascading section of the blue shift.

The increase in the maximum intensity of the $I_{\max}$ PL from t_f in Figure 2, *c* is attributable to an increase in the thickness of PS. The acceleration of this growth is probably due to the heterogeneity of the pore density. In regions with reduced pore density, with an increase in their diameter, oxidation leads to the formation of new quantum silicon filaments, which make an additional contribution to PL.

There are six known models for explaining PS PL [1, section 5.3]. In addition to the quantum-dimensional model of radiative recombination in the volume of a nanoscale fragment of a silicon quantum wire in a PS, all other models are related to the PL of external formations on the surface of a silicon filament (hydrogenated amorphous silicon, surface hydrides, surface defects, surface molecules, surface states). A recent article [14] notes the lack of consensus on the nature of PL in PS. As mentioned above, with increasing thickness of the porous layer, its porosity increases, therefore, with increasing pore diameter, the specific area of the total surface of silicon filaments decreases. This means that the surface model should lead to a sublinear dependence of the PL intensity on the formation time t_f of PS layers. The experimentally observed superlinear increase in PL intensity from t_f in Figure 2, *b* indicates in favor of a volumetric quantum-dimensional model.

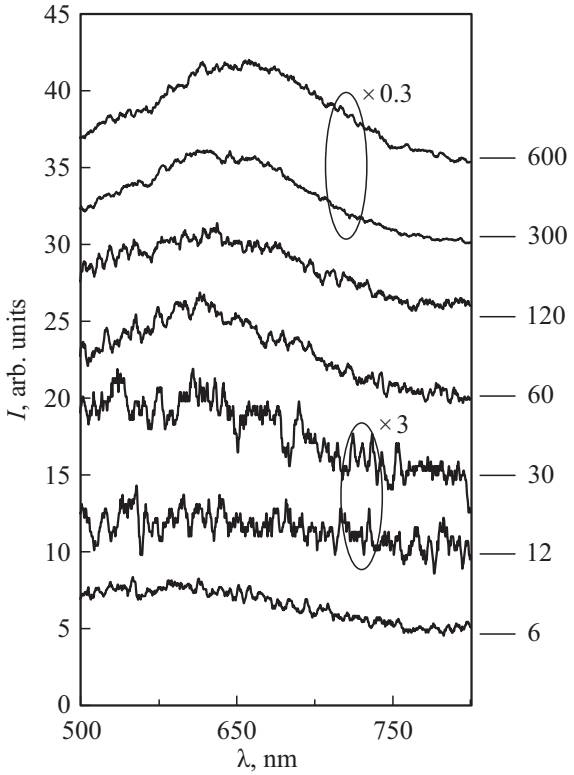

Figure 4. PL spectra of PS samples on KES-0.01 at 293 K for different formation times t_f, shown by the numbers on the right in seconds.

There are common features of the PL spectra of PS and silicon nanoparticles embedded in silicon oxide SiO_2. In both cases, the aforementioned S-band, F-band, IR-bands, and the hot photoluminescence (Hot PL) band considered in the case of silicon nanocrystals [1,2,11,15,16] were observed. The F-PL band at 420–470 nm weakly depends on the size of Si nanoparticles, is attributed to defects and impurities in silicon oxide, is characterized by a low quantum yield of up to 0.1 %, and lies outside the measurement range in Figure 1. The IR band 1100–1500 nm is associated with states at the Si-SiO_2 boundary, presumably broken silicon bonds and is located outside the range of our measurements in Figure 1. Hot PL 425–603 nm is described in the model of quantum confinement in silicon nanocrystals, is characterized by direct interband transitions, is characterized by an unusual PL redshift for quantum confinement with a decrease in the size of nanocrystals, very low quantum efficiency, much lower than that of PS, and the need for a very high level of excitation, far from the one used in this study.

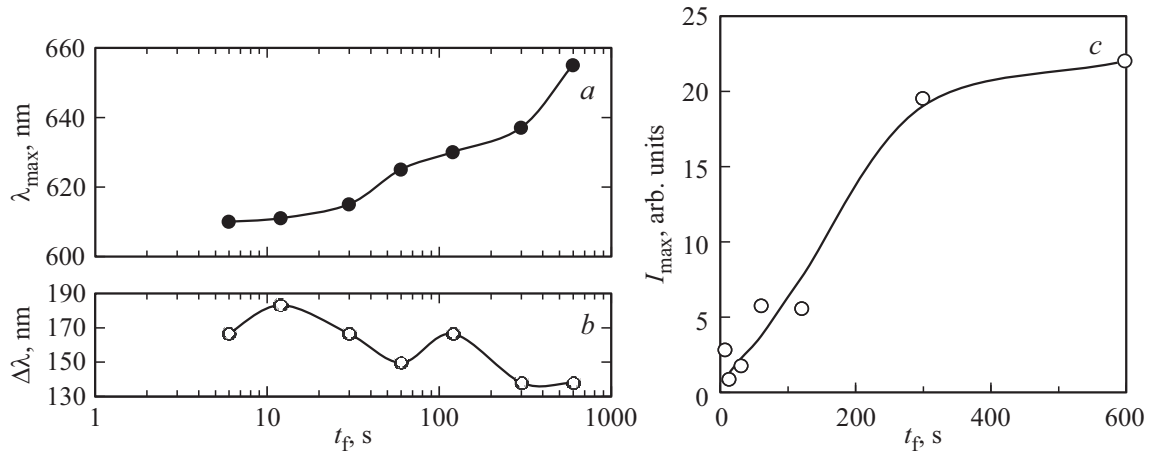

Figure 5. Dependences of the parameters of the PL spectra at 293 K on the formation time t_f of PS layers on single crystals KES-0.01: *a* — positions of the PL maximum λ_{max}, *b* — spectral widths $\Delta\lambda$, *c* — maximum PL intensity I_{max}.

We also note the volumetric luminescence centers associated with dislocations in silicon [17,18,19]. This is a family of so-called D1-D4 lines, at wavelengths at low helium temperatures of 1524, 1414, 1314 and 1236 nm, respectively. However, these lines are located far in the infrared region of the spectrum, and it is rather impossible 2−2.5 to shift them by a factor of blue into the region of the studied visible PL spectrum of the PS. The most intense lines D1, D2 are associated with point defects near dislocations, weakly depend on a change in the band gap of silicon and decrease in amplitude by two orders of magnitude with an increase in temperature to 300 K. These point defects are deep centers with an electron localization radius of the order of the interatomic distance 0.2 nm and their state is unlikely to change significantly when externally limited to a region with a diameter of ~ 2 nm.

Thus, only the quantum confinement model for the PL S-band is relevant in our analyses of the PS PL data on KDB-2 in Figure 1. The same applies to the PS PL data on KES-0.01 below in Figure 4.

Figure 4 shows the PL spectra of PS samples on KES-0.01 at 293 K for different times t_f of formation of porous layers with increased spectrometer gain by one hundred times compared with the data in Figure 1 for KDB-2. As in the case of KDB-2 in Figure 1, it was possible to observe the PL of PS samples with a change in the formation time by two orders of magnitude from 6 s to 600 s, which, in the approximation of linear thickness growth d_{PS} of PS corresponds to a change in d_{PS} from 20 nm to 2000 nm.

The dependences obtained from the spectra of Figure 4 on the formation time t_f of PS layers on single crystals KES-0.01 of the position of PL maximum λ_{max}, the width of the PL line at half height $\Delta\lambda$ and the PL intensity I_{max} are shown in Figure 5. As in the case of KDB-2, there is a red shift of the PL maximum and an increase in intensity I_{max}, but with a slowdown after $t_f = 300$ s, as the thickness of the porous layer increases. As in the case of PS on KDB-2, there are signs of a cascading mechanism for the growth of PS layers on KES-0.01. Sections with positive and negative curvature alternate on the curve $\lambda_{max}(t_f)$, Figure 4, *a*, and on Figure 4, *b*, at least up to $t_f = 120$ s, there are antiphase changes $\Delta\lambda(t_f)$.

As in the case of PS on *p*-Si, the nature of PL and the mechanism of formation of a nanoscale PS are possible within the framework of the dimensional quantization model. Nanoscale silicon filaments are formed, the transverse size of which determines the wavelength λ_{max} of the PL maximum. The range of variation of λ_{max} 610−655 nm is somewhat narrower here than in the case of KDB-2 (600−697 nm), but of the same order. This means that the resulting quantum filaments in the PS on KDB-2 and KES-0.01 have a similar cross-section. The slowdown in the growth of I_{max} after $t_f = 300$ s in Figure 5, *b* as the thickness of the porous layer increases may be due to the presence of a space charge region in silicon near the silicon−electrolyte boundary. The difference between the mechanism of PS layer growth on Si-n^+ is that the holes on the silicon−electrolyte boundary are supplied not from bulk silicon, but from the region of spatial charge, where they are generated as a result of electrical breakdown of this region. Silicon KES-0.01 with a resistivity of $0.01\,\Omega\cdot$cm corresponds to the concentration of donors of $5\cdot 10^{18}$ cm^{-3}, the Debye shielding length is about 2 nm [20]. This means that the space between the pores is narrowed by the spatial charge regions and the holes are limited for electrotransference.

Figure 6 shows a family of EPR spectra of PS layers on KES-0.01 at 293 K. The EPR spectrum of the known [1,19]P_b-centers of nonradiative recombination was observed in the entire range of t_f from 6 s to 600 s. The presence of these spectra indicates the presence of silicon nanoparticles in the PS; oxidation in air, in accordance with the PL data, did not lead to the complete transformation of silicon inclusions into silicon oxide. As it turned out, the amplitude of these spectra Y' depends almost linearly on the time of PS formation (Figure 7).

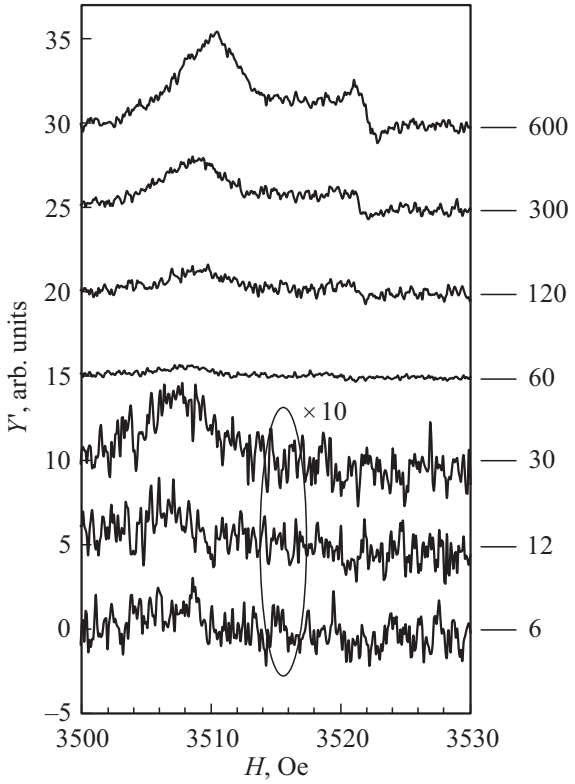

Figure 6. A family of EPR spectra of PS layers on single crystals KES-0.01, measured at 293 K.

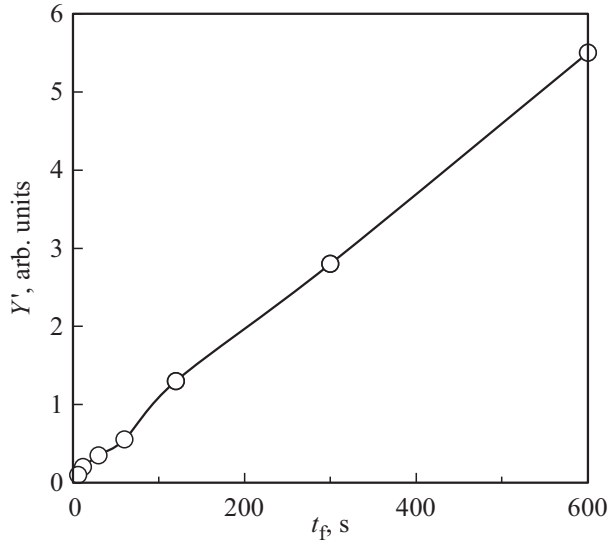

Figure 7. Dependence of the amplitude Y' of the first derivative of the EPR absorption spectrum of P_b-centers on the time of formation of PS on KES-0.01.

If we assume that the thickness of the PS layer increases linearly with the formation time, the linear graph in Figure 6 means a uniform distribution of P_b-centers over the volume of the PS layers, regardless of their thickness. Arguments were made in Ref. [19] that the nature of the P_b-centers is not related to broken bonds at the Si-SiO_2 interface, but to internal defects suggested by dislocations in silicon nanoclusions in PS. The experimentally observed linear increase in PL intensity from t_f in Figure 7 indicates a close to linear increase in the total mass of silicon filaments with an increase in the thickness of the PS layer on Si-n^+.

It should be noted that the two orders of magnitude weaker PS glow on Si-n^+ compared to Si-p is attributable to two circumstances. Firstly, the position of the Fermi level in silicon with a high content of small donors is unfavorable for PL, and secondly, the same position of the Fermi level is favorable for the manifestation of P_b-centers suppressing PL.

It was suggested in Ref. [12] that due to the enormous mechanical stresses during PS oxidation, silicon filaments probably break into fragments with a length of one to several diameters, as schematically shown in Figure 7 in Ref. [21]. The enormous stresses are caused by the fact that, as mentioned above, the volume of silicon oxide formed is twice the volume of the original silicon. The gaps between the fragments of the filament are filled with silicon oxide. That is, according to the above-described model of both PL and the formation of a nanoscale PS, in fact, we observed PL from PS with torn quantum wires—garlands consisting of segments of silicon filaments and silicon granules embedded in silicon oxide. According to the data of the band gap of quantum wires [1, tabl. 4], exciton energy depends on the size of the nanocrystal [15 Figure 3] and according to Ref. [11] estimates of the maximum PL position depending on the diameter of the filaments and granules are close. So the above estimate of the diameter of the filaments at 2 nm is also suitable for the diameter of silicon granules in a PS. Obviously, all of the above arguments about the redshift of PL are applicable to fragments of broken silicon filaments.

A recent article [22] talks about the current technology for manufacturing a system of silicon nanowires (NWs) immersed in a dielectric medium. In the light of what is described in this article, we can propose a technology for manufacturing such NWs systems from PS. As mentioned above, silicon nanowires formed in PS during its oxidation are torn by mechanical stresses. It is probably possible to avoid the rupture of silicon filaments by a multi-stage process of PS oxidation and dissolution of the oxide in hydrofluoric acid. At the same time, each oxidation stage should be short enough in time to prevent breaks in the silicon frame of the PS and then in the silicon nanowires in the PS. At the end, the gaps between the nanowires are filled with a kind of dielectric, which prevents further oxidation of the nanowires and ensures the mechanical strength of the NWs structure.

Conclusion

The effect of the anode formation time of t_f from 6 s to 600 s on photoluminescence and electron paramagnetic resonance of porous silicon on single crystals of p- and n^+-type has been studied. For the first time, photoluminescence and electron paramagnetic resonance were observed

on ultrathin layers of porous silicon on Si-p with a thickness from 10 nm and on Si-n^+ with a thickness from 20 nm. As a result of air oxidation, nanoscale silicon filaments surrounded by silicon oxide are formed in porous silicon. According to photoluminescence data, the cross-sections of silicon filaments in porous silicon on p- and n^+-type single crystals are similar in size, with a diameter of about 2 nm. A cascade quantum-dimensional mechanism of mesaporous silicon growth is proposed, which explains the red shift of photoluminescence with increasing PS porosity. Due to the enormous mechanical stresses during PS oxidation, silicon filaments are torn into fragments ranging in length from one to several diameters. This does not negate the proposed quantum-dimensional mechanism of mesaporous silicon growth and the explanation of the redshift of PL. According to the data of the electron paramagnetic resonance of P_b-centers, the total mass of silicon fragments of broken nanowires in the PS layer increases almost linearly with an increase in the thickness of this layer on Si-n^+. The possibility of developing a technology relevant today for manufacturing a system of silicon nanowires immersed in a dielectric medium is discussed.

Conflict of interest

The authors declare that they have no conflict of interest.

References

[1] O. Bisi, S. Ossicini, L. Pavesi. Surf. Sci. Rep. **38**, 1 (2000).
[2] Handbook of Porous Silicon, Leigh Canham Editor, Springer International Publishing Switzerland (2014). 1012 p.
[3] V.V. Tregulov. Vliyanie osobennostej formirovaniya plenok poristogo kremniya na harakteristiki poluprovodnikovyh bar'ernyh struktur. Avtoref. dokt. diss., RGU im. V.F. Utkina, Ryazan' (2022). p. 39 (in Russian).
[4] A.S. Lenshin, V.M. Kashkarov, P.V. Seredin, B.L. Agapov, D.A. Minakov, V.N. Tsipenyuk, E.P. Domashevskaya. Tech. Phys. **59**, 224 (2014).
[5] X.G. Zhang. J. Electrochem. Soc. **138**, 3750 (1991).
[6] V. Lehmann, H. Fôll. J. Electrochem. Soc. **137**, 653 (1990).
[7] S. Matthias, F. Muller, J. Schilling, U. Gösele. Appl. Phys. **A80**, 1391–1396 (2005).
[8] S.J. Gregg, K.S.W. Sing. Adsorption Surface Area and Porosity. Academic, N.Y. (1982).
[9] L.T. Canham. Appl. Phys. Lett. **57**, 1046 (1990).
[10] N. Ennejah, S. Aouida, B. Bessais. Phys. Status Solidi **C8**, *6*, 1931 (2011).
[11] L.T. Canham. Faraday Discuss. **222**, 10 (2020).
[12] E.S. Demidov, A.S. Abrosimov, N.E. Demidova, V.V. Karzanov. Phys. Solid State **61**, 285 (2019).
[13] A.J. Read, R.J. Needs, K.J. Nash, L.T. Canham, P.D.J. Calcott, A. Qteish. Phys. Rev. Letters **69**, 1232 (1992).
[14] A.V. Kozhemyako, A.A. Shemukhin, A.V. Nazarov, Yu.M. Spivak, E.N. Muratova, V.V. Chernysh. VMU. Seriya 3. Fizika. Astronomiya **6**, 69–74 (2020) (in Russian).
[15] O.B. Gusev, A.N. Poddubny, A.A. Prokofiev, I.N. Yassievich. Semiconductors **47**, 182 (2013).
[16] W.D.A.M. de Boer, D. Timmerman, K. Dohnalova, I.N. Yassievich, H. Zhang, W.J. Buma, T. Gregorkiewicz. Nature Nanotechnology **5**, 878 (2010).
[17] N.A. Sobolev. Semiconductors **44**, 1–23 (2010).
[18] V. Kveder, M. Kittler. In: Advances in Light Emitting Materials, ed. by H.G. Grimmeiss, B. Monemar, M. Kittler, ch. 3. Mater. Sci. Forum **590**, 29 (2008). (Trans. Tech. Publications, Switzerland, 2008)
[19] N.E. Demidova, E.S. Demidov, V.V. Karzanov. Phys. Solid State **63**, 449 (2021).
[20] S. Zi. Fizika poluprovodnikovykh priborov. Mir, M. (1984). p. 28, 85. (per. s angl. S.M. Sze. Physics of Semiconductor Devises, 1981).
[21] N.E. Demidova. Avtoref. kand. dis. NNGU im. N.I. Lobachevskogo, Nizhnij Novgorod (2010). p. 18 (in Russian).
[22] Manuel F. Gallego, Rosa M. de la Cruz, Clément Kanyinda-Malu. Academia Nano: Science, Materials, Technology **2**, *2*, 1-12 (2025).

Translated by A.Akhtyamov